



Modeling water purification by an aquaporin-inspired graphene-based nano-channel

A. Lohrasebi^{1,2} · T. Koslowski³

Received: 3 April 2019 / Accepted: 14 August 2019 / Published online: 28 August 2019
© Springer-Verlag GmbH Germany, part of Springer Nature 2019

Abstract

Understanding the mechanism of water and particle transport through thin-film membranes is essential to improve the water permeability and the salt rejection rate of the purification process. In this research, mimicking from the structure and operation of the aquaporin channel, graphene-based nano-channels were designed to be used as a water filter. The effects of variation of the channel's main elements, such as the width of the bottleneck and charges attached to the channel on its efficiency, were investigated via molecular dynamics simulations. We observe that the water flow through the channel decreases by increasing the charge, while the ion rejection rate of the channel is enhanced. Moreover, we find that the geometry and shape of the bottleneck part of the channel can affect the channel water flow and its selectivity. Finally, the pressure and the flow velocity in the channel were considered by using finite element models, and the results indicate that they are high at the entrance of the channel. The outcomes of this study can be used to improve the molecular knowledge of water desalination, which might be helpful in designing more efficient membranes.

Keywords Water desalination · Aquaporin · Graphene-based channel · Molecular dynamics simulation

Introduction

According to the lack of fresh water resources, there is a crucial need for improvement of low-cost technologies for water distillation enabling access to safe drinking water for people especially in the developing countries. As a practical approach, water-filtering processes can be used to overcome this challenge, and since most of the biological cells have the ability of water filtering, water desalination could be performed with the aid of nano-filters designed to mimic the biological filters of cells, such as

aquaporins. Aquaporins are **integral membrane proteins** that form **channels** in the **biological cell membrane**, through which **water** can flow rapidly into and out the **cell**, without the passage of any ions [1, 2]. Hence, mimicking their structure and function could be very helpful in designing high-performance micro- or nano-filters. So far, their structural dynamics and the mechanism of water molecule transport have been investigated in several studies [3–6]. It was reported that the hourglass shape of the aquaporin channels facilitates fast water transport through the cell membrane with no leakage of ions. Furthermore, it was found that the aquaporins act as a two-stage filter. The first stage of the filter is located in the central part of the channel (NPA); and the second one is placed on the external cellular face of the channel (ar/R) [3, 7]. Moreover, the electric field created by the special arrangement of amino acids within the NPA region is supposed to be a main factor in proton rejection and water permittivity through aquaporin [3, 6, 7]. The structure of these kinds of channels is shown schematically in panels of Fig. 1.

Inspired by the operation and function of the protein channels, such as aquaporins and ion channels, artificial nano-scale filters can be proposed to use in various

Electronic supplementary material The online version of this article (<https://doi.org/10.1007/s00894-019-4160-y>) contains supplementary material, which is available to authorized users.

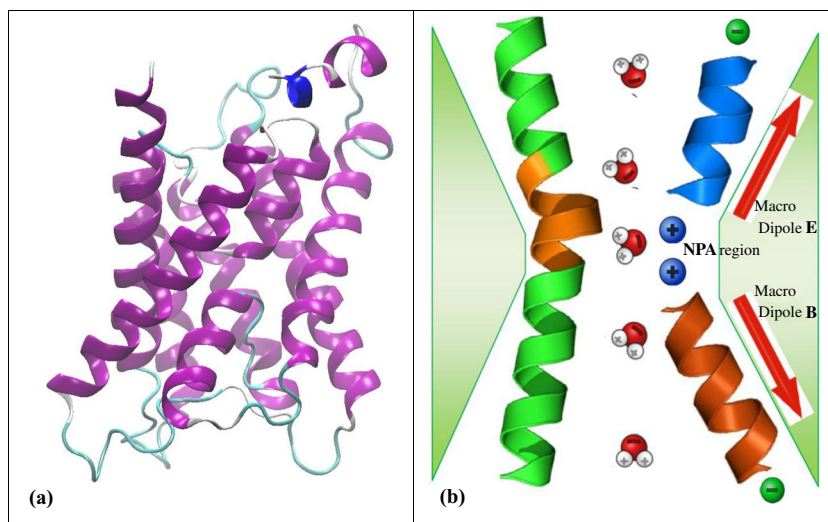
✉ A. Lohrasebi
lohrasebi@nano.ipm.ac.ir

¹ Department of Physics, University of Isfahan, Isfahan 8174673441, Iran

² School of Nano-Science, Institute for Research in Fundamental Sciences (IPM), Tehran 193955531, Iran

³ Institute for Physical Chemistry, University of Freiburg, Albertstrasse 23a, D-79104 Freiburg, Germany

Fig. 1 The schematically view of main facial appearance of aquaporin channel. **a** The structure of AQP0 channel-based 2b6o-pdb code. **b** The hourglass shape of aquaporin channel



applications of nano-technology. For this purpose, carbon nano-structures are usually used to design nano-scale devices, such as nano-motors [8], nano-pumps [9–11], and nano-filters [12, 13]. On the other hand, designing and modifying thin-film membranes made from carbon materials, which can be employed in reverse osmosis (RO) pressure-driven processes, have been the subject of recent computational and experimental studies [14–20]. Recent investigations have indicated that the physical and chemical properties of nano-membranes are important factors that affect the passage of water molecules through the channels [21, 22]. For example, Cohen-Tanugi et al. [18] have shown that water flow through the graphene membrane can be controlled significantly by the variation of the hydrophilic or hydrophobic behavior of the porous graphene. In other studies, the consequences of the channel structural parameters on the water flow through a graphene membrane have been studied theoretically and by computer simulations [19, 23, 24].

Strong confinement of water molecules in structures such as carbon nano-tubes (CNTs) substantially modifies the structural, thermodynamic, and dynamic properties by changing the structure of the hydrogen bond network. In this regard, Chakraborty et al. provided an overview of the behavior of confined water inside CNTs and between graphene and graphene oxide (GO) sheets, computationally [25]. Their results demonstrate that water molecules confined in short and narrow CNTs with open ends exhibit Fickian diffusion because of their collective motion. Furthermore, they showed that the potential of mean force for the oxidized part of GO sheets in the presence of water exhibits two local minima, corresponding to a dry cavity and the fully hydrated cavity. Recently, Giri et al. investigated the effects of oxidation degree and interlayer spacing on the filtration efficiency and water structure in graphene oxide (GO) via the application of molecular dynamics

(MD) simulations. They showed that the water permeation increased by increasing interlayer separation (the best amount was 0.8 nm) and decreased with increasing oxidation degree (the best value was 10% or lower) [26]. In the other computational study based on the MD simulation method, they examined the dependence of the structure and dynamics of confined water on the diameter and length of the capped carbon nano-tubes (CCNTs) [27]. Their results indicated that the water density reduced along the capped side of the CNTs, and the average density of hydrogen bonds decreases with increasing length of the CCNT and decreasing diameter.

Using molecular dynamics simulations, it was shown that the electrical charges of the nano-pore edge can be used to increase the salt rejection rate of the membrane [3]. Experimentally, the water permeability variation was measured by considering the effects of graphene sheet alignment and membrane hydrophobicity [28, 29]. In the other investigation, a water nano-pump driven by a vibrating charge was examined by using MD simulations [30]. The simulation results indicated that the CNT radial deformation plays a key role in pumping water molecules through the CNT and showed that the water flux increased linearly by increasing the CNT deformation up to a critical value, and above that decreases sharply.

In our work, a graphene-based nano-channel is designed for water purification, which is inspired by the structure of aquaporins. The effects of different channel structural parameters on its operation have been considered by employing MD simulations. The results indicate that the transport of water molecules and salt ions is seriously influenced by changing the parameters underlying the model, such as the charges attached to the channel, and that the channel operation can be optimized with respect to these parameters. The results of this study could be helpful for designing high-efficiency membranes used in water treatment procedures.

Molecular models and simulation details

Our computational approach is an atomistic one, embodying a geometry that captures the major physical details, such as channel position and width and the location and amount of charges. While chemical realizations of a channel may look different in detail, we intend to introduce a model that describes the relevant parameters of the system and a representation that is as reduced and transparent as possible. Our simulation strategy is motivated by pressure-induced flow measurements on aquaporin [31] and micrometer-sized channels in graphene [13, 32]. We note that the length scales that we inspect are considerably smaller than those studied in ref. 13 and that they have a crucial impact on capacity and selectivity, as will be demonstrated below.

The computational setup was made of a graphene-based nano-channel of 10 Å height and a length of 30 Å, which consists of two graphene sheets aligned in parallel in the z -direction. To create a bottleneck within the channel, as inspired by the aquaporin hourglass shape, an additional small graphene layer of dimensions of $10 \times 25 \text{ Å}^2$ was located in the channel, as it is shown in Fig. 2. Ten immobile cations and anions were attached to the channel around the bottleneck area. According to the location of the attached charges and the bottleneck, three different structures were designed (models 1–3), which are schematically shown in the panels of Fig. 2. In addition, two water reservoirs were placed on both sides of the channel (box I and box II). The geometry lengths are shown in Fig. 2. For each geometrical arrangement, the magnitude of the charges is varied.

In all of the simulations, the box I was initially full of a solution (water molecules, Na^+ and Cl^- ions) with a salinity of 35 g/l and a density of 1 kg/l. Then, the solution was pushed toward the nano-channel by applying a pressure of 0.2 atm with the aid of a rigid piston made of an additional graphene sheet. To carry out the simulations the LAMMPS package [33] in the NVT ensemble was used, in which the Nosé-Hoover thermostat was employed to maintain the temperature at $T = 300 \text{ K}$. The velocity-Verlet method was utilized to integrate the equations of motion of the particles in the system, and periodic boundary conditions were imposed in the simulations. The intermolecular interactions between carbon atoms in the graphene sheet were calculated with the adaptive intermolecular reactive empirical bond-order (AIREBO) potential [34], and the transferable intermolecular potential 4-point (TIP4P) model [35] was used to compute the water molecule interactions. The Lennard-Jones (LJ) potential was considered to describe the non-bonding interactions between water molecules-carbon atoms and water molecules-attached charges. The Lorentz-Berthelot mixing rule was employed for cross-interactions, and the related parameters are listed in Table S-1 [36] of supplementary materials. In all simulations, carbon atoms and the attached charges were fixed. Moreover,

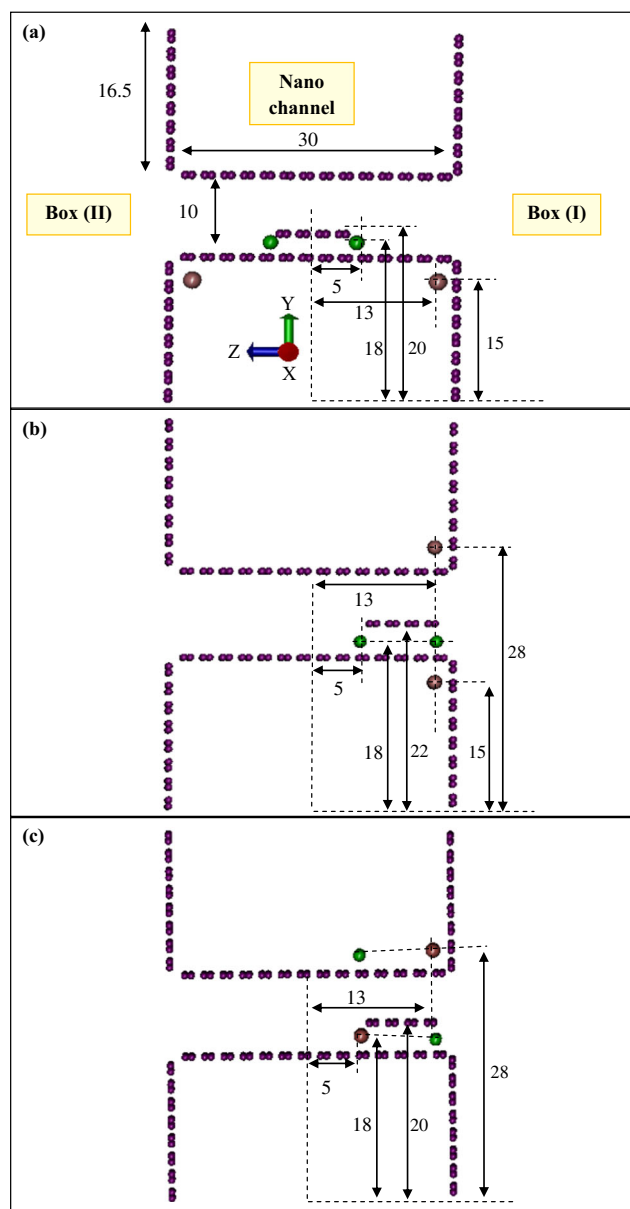


Fig. 2 The structure of the designed system components for three models, in which the attached positive and negative charges are highlighted respectively as green and pink spheres. **a** Side view of the channel in model 1. **b** Side view of the channel in model 2. **c** Side view of the channel in model 3. Unit of the presented lengths is angstrom

electrostatic interactions were computed by the application of the particle-particle particle-mesh (PPPM) method. A cutoff radius of 12 Å was used to calculate the Van der Waals and Coulombic interactions.

In all simulations, following the equilibration, several simulations of the period of 2 ns were performed, to examine the influence of some channel structural parameters, such as the locations and the amount of the attached charges, on the nano-channel performance. In all cases, the simulation time turned out to be sufficient to observe a stationary flow of water molecules and salt ions through the channel.

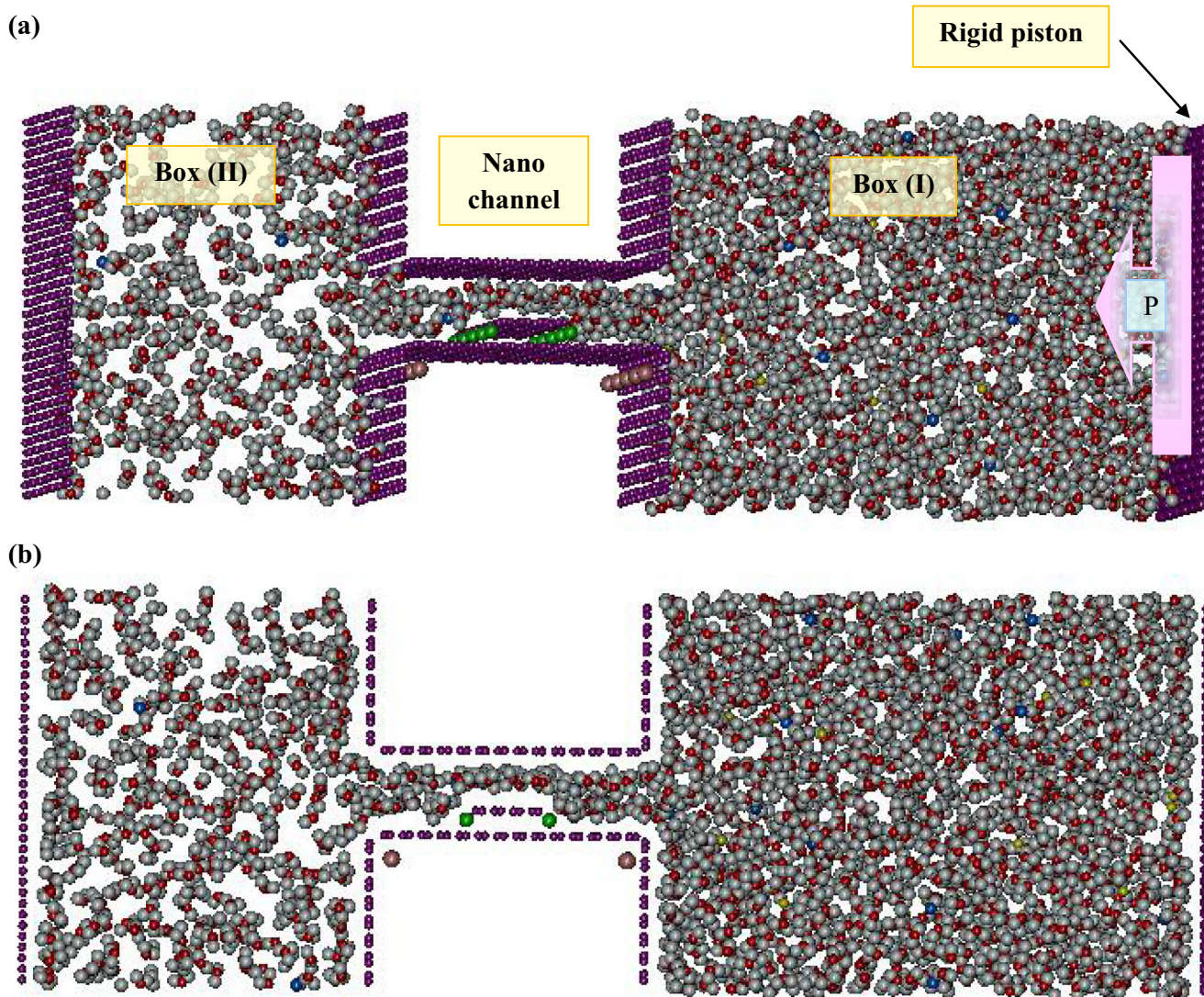


Fig. 3 The structure of the designed system for model 1: **a** 3-D view and **b** 2-D side view of the simulated system after 200 ps

While the atomistic molecular dynamics simulations are well suited to address the question of water and ion migration, we also wished to have a look at the hydrodynamic properties of the fluid within the channel. Here, we have considered a numerical, finite element solution of the Navier-Stokes equations appropriate to compute important parameters such as the flow velocity, the pressure profile, and the surface stress, which may affect the mechanical integrity of the nano-channel. These computations have been performed with the help of the COMSOL-Multiphysics software version 5.3.1 [37].

Results and discussion

We now turn to the numerical results of the impact of the different structural parameters of the graphene-based nano-channel on water and ion transport. We study three different models; all are variants of the geometry displayed in Fig. 2. They comprise a combined element of a bottleneck and charges, which is located within the channel. For the first model, this structural element is placed in the middle of the channel, but is moved toward its entry for the second model.

Table 1 The average percent of rejected ions and water flow through the channel for model 1

| Ion rejection (%) for a NaCl solution for the first structure (model 1) | | | | |
|---|----------------|-------------------|-----------------|-----------------|
| | $q = q' = 0.0$ | $q = -q' = -0.5e$ | $q = -q' = -1e$ | $q = -q' = -2e$ |
| Ion rejection percent | 48.2 | 59.5 | 71.4 | 80.9 |
| Water flow ($\text{dm}^3/\text{s cm}^2$) | 0.409 | 0.406 | 0.405 | 0.399 |

Table 2 The average percent of rejected ions and water flow through the channel for model 2

| Ion rejection (%) for a NaCl solution for the second structure (model 2) | | | | |
|--|----------------|-------------------|--------------------|-----------------|
| | $q = q' = 0.0$ | $q = -q' = -0.5e$ | $q = -q' = -0.75e$ | $q = -q' = -1e$ |
| Ion rejection percent | 78.6 | 90.5 | 92.8 | 95.2 |
| Water flow (dm ³ /s cm ²) | 0.277 | 0.276 | 0.274 | 0.265 |

Model 3 differs from model 2 by the arrangement of the charges: they are located on one side of the bottleneck for the further, while half of them are moved toward the opposite wall of the channel for the latter.

To obtain a better understanding of the nano-channel operation, a typical simulation procedure of water filtering by our designed channel is described in the following. Figure 3 shows the snapshot of the overall simulation process following equilibration after 200 ps for model 1. The solution in box I is pushed along the z-direction of the simulation box, toward the channel via the application of the piston. The water can now flow through the channel, while most of the salt ions cannot pass through the bottleneck of the channel, since the ion hydration radius is usually larger than the narrowest part of the channel (the hydration radii of Na⁺ and Cl⁻ are about 3.6 and 3.3 Å, respectively [38]). Therefore, only dehydrated ions can pass the channel, and as the reservoir generally cannot deliver the required dehydration energy, most of the ions remain in box I.

In addition, the attached positive and negative charges which are located inside the channel usually prevent the passage of Na⁺ and Cl⁻ ions. The charges generate an electric field inside the channel, which in turn induces a potential barrier for the salt ions. Hence, increasing the amount of charge attached to the channel with a suitable arrangement causes salt ions to enter box II with a smaller probability. However, in the majority of simulations, the water flow through the channel is also reduced upon the introduction of charges, so we have to define relative measures of ion rejection and water flow. They are defined as $(\frac{\text{number of ions} - \text{number of passed ions}}{\text{number of ions}} \times 100)$ and (linear slope of the number of passed water molecules through the channel as a function of the simulation time), respectively. In Tables 1, 2, and 3, the corresponding numerical values are reported for the three models employed here.

From these data, it is evident that increasing the amounts of attached charges at the channel entry increases the ion rejection, while it decreases the water flow rate for models 1 and 2. For

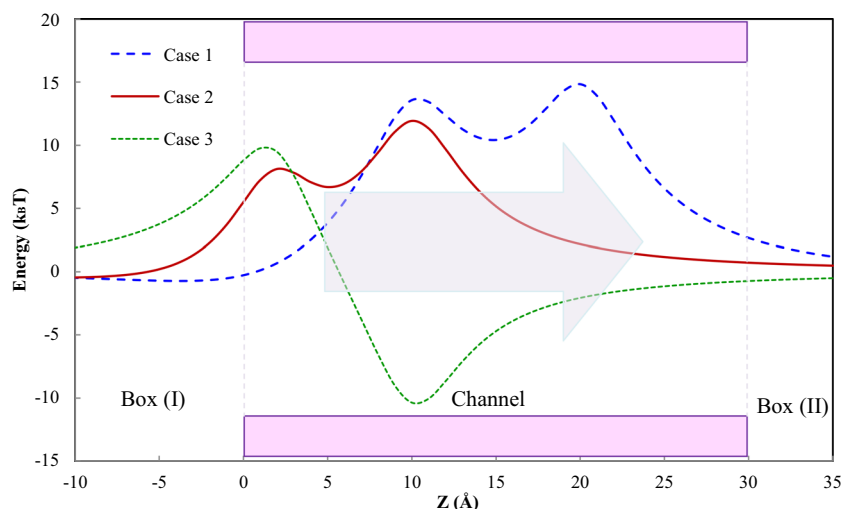
model 3, on the other hand, both values are increased by increasing the charge. This behavior might be due to the arrangement of the attached charged in the channel, which induces different potential barriers for the ions entering the channel. These potential barriers could lead to decrease the number of ions passing the membrane. Considering this point, the potential energy profiles derived from electrostatic interactions between the salt ions and attached charges ($q = 1e$) were calculated along the z-direction of the channel for the three models studied. To compute the potential energy profiles, a test charged was moved through the channel in vacuum. The results are shown in Fig. 4, and as it can be seen, the potential barriers for the entrance of ions into the channel are higher for models 2 and 3 than they are for model 1. Furthermore, the potential barrier of model 2 is considerably broader than this value of model 3 counterpart. This may reduce the probability of ion passage through the channel for model 2, which is in accord with the data of Tables 1 and 2. Hence, we conclude from these results that the channel with the configuration of model 2 constitutes the most suitable design of the three introduced here, since it has the highest tendency toward ion exclusion for a given charge of $q = 1e$ attached to the channel.

In addition, since the water molecules constitute microscopic dipoles, they are influenced by the electric field generated from the charges attached to the channel walls. In fact, the electric field line pattern could affect the water molecule orientations and their motion inside the channel, and so, water flow rate through the channel could be influenced by the charge arrangements in different cases (the related schematic figures for model 2 are presented in panels of Fig. S-1, in supplementary materials). To show this, the water molecule orientations were calculated by computing the angles between the water dipoles and the z-direction of the channel. The averages of water molecule orientations, when they passed through the channel, are shown in Fig. 5, for three different values of attached charges to the channel of case 2. As can be seen, the orientations of water molecules changed (tend to

Table 3 The average percent of rejected ions and water flow through the channel for model (3)

| Ion rejection (%) for a NaCl solution for the third structure (model 3) | | | | |
|---|----------------|-------------------|--------------------|-----------------|
| | $q = q' = 0.0$ | $q = -q' = -0.5e$ | $q = -q' = -0.75e$ | $q = -q' = -1e$ |
| Ion rejection percent | 78.6 | 85.7 | 90.5 | 92.9 |
| Water flow (dm ³ /s cm ²) | 0.263 | 0.262 | 0.268 | 0.276 |

Fig. 4 The schematic view of the potential barrier energy profiles inside the channels for different cases

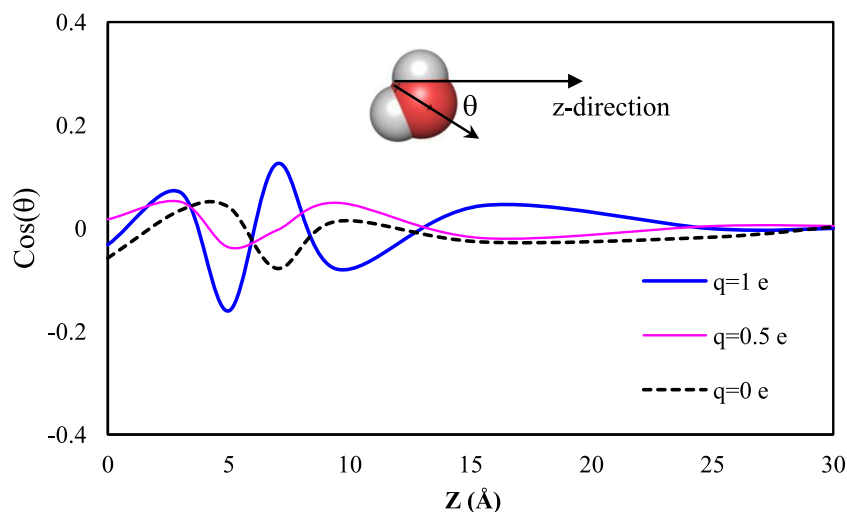


align along the electric field created by the charges attached to the channel walls) during the passage through the narrow part of the channel, mainly for the large amount of the attached charge. In some of previous studies, it was reported that water molecule orientations influenced during the passage through the nano-channels [26] and when electric fields applied on the channels [20]. Therefore, both the water flow through the channel and the ion rejection rate depend on the charge arrangement in the channel.

Our findings and interpretations are in agreement with those obtained for the biological system that inspired us [3, 6, 7]. They indicated that in the aquaporin channels, proton rejection and water permeation are enabled by the electric field generated by the partial charges of NPA region and the macro-dipoles of the B and E helices of the protein; these elements are highlighted in Fig. 1.

On the other hand, we find that the channel performance is related to the width of the bottleneck, i.e., the part of the channel that contains the small graphene sheet, and that it can be regulated by moving this sheet along the y -direction.

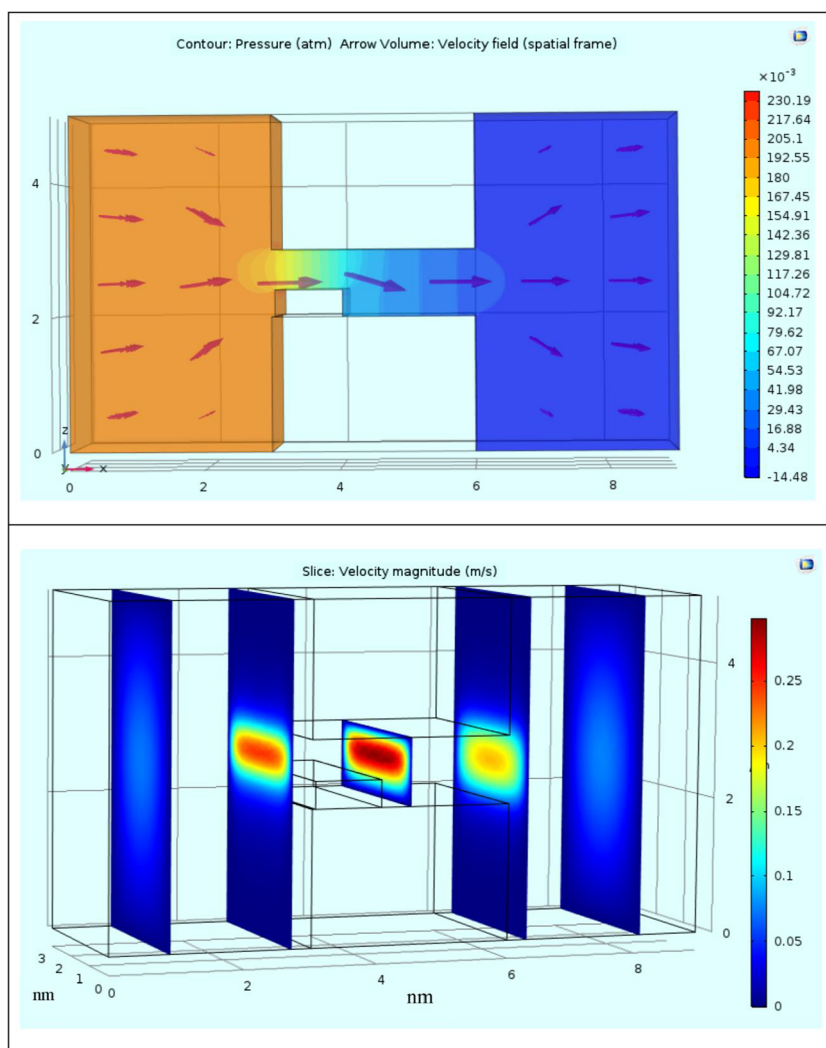
Fig. 5 The averages of water molecule orientations in the channel, for three different values of attached charges to the channel of case 2



We observe that the water flow is reduced by decreasing the width of the bottleneck, while simultaneously rejecting more ions (the related data are listed in Tables S-2 and S-3, in supplementary materials). Thus, both the water permeability and the selectivity of the channel can be tuned, but not independently. To make it more clearer, it is worth mentioning that the permeability of the natural aquaporin was observed to be about 10^8 – 10^9 water/s/channel with perfect rejection of ions and protons [39, 40], while these parameters for our designed channels are in the range of 10^{12} water/s/channel and 85–93%, respectively. Furthermore, it was reported in several studies that water transport within subnanometric CNTs with the diameter in the range of 1 nm embedded into lipid environments exceeds that of biological AQP water transporters up to an order of magnitude [41, 42].

We finally turn to the results obtained by the finite element model of the channel. As referenced above, the Comsol software package was used to describe the nano-channel in order to understand the flow and the mechanical parameters of the water purification process. For this

Fig. 6 **a** The volumetric velocity field arrows and pressure inside the system. **b** Five planes of velocity profile inside the system for case 1, in the steady-state condition



purpose, we have used structures as similar as possible to the atomistic models. They are devoid of the atomistic roughness of the channel, but share the parameters depicted in Fig. 2b. We have studied laminar flow with boundary conditions appropriate to this regime; the systems were modeled in the steady state. The volumetric velocity field arrows and pressure inside the system for model 2 are shown in the first panel of Fig. 6, and five planes of velocity profile are presented in the second panel. It can be observed that the applied pressure and the flow velocity in the entrance of the channel are very high, which could supply the required dehydration energy of salt ions in this area.

Therefore, the mechanism of ion dehydration by thermal energy (which related to the kinetic energy of particles) deserves further attention. To clarify this issue, we briefly describe the overall dynamics of the ions in the simulated system. Most of the hydrated ions in the box I cannot pass through the channel because at first, they must be dehydrated to pass the narrow part of the channel and

in addition, they should be able to overcome the potential energy barrier that is created by the repulsive interaction between the ions and attached charges to the channel (it is shown in Fig. 4). As can be seen, the potential energy barrier for entering a Na^+ ion into the narrow part of the channel for case 2 is in the range of $12 k_B T \approx 0.3 \text{ eV}$ and the required energy for NaCl ions dehydration is about 4 eV [43]. As it was mentioned above, the flow velocity in the entrance of the channel is very high (Fig. 5), which leads to increase the temperature of this area and therefore when ions close to the channel entrance area, the probability of transferring the ions entering required energy to the channel (dehydrated and overcome the potential energy barrier) from the surrounding aqueous medium is increased. This phenomenon may reduce the selectivity of the filter, i.e., by increasing the applied pressure on the salt solution in box I, the channel selectivity will be decreased, as the probability of ion dehydration is increased. A similar result was obtained in our previous study [12].

Conclusions

Inspired by the function and structure of the aquaporin water channel, we have designed models of graphene nano-channels that mimic the protein. The main element of our model is a bottleneck supplemented by ionic charges. The influence of the geometry and charge on the function and operation of graphene-based nano-channels was studied by atomistic molecular dynamics simulations.

We have found that, as far as the attached charge was concerned, the water flow through the channel was reduced by enhancing the amount of the charge, while the selectivity (ion rejection) was increased. This behavior can be rationalized by considering the potential barrier energy in the channel and electric field line pattern. In addition, we find that the water flow and the ion rejection percentage depend on the channel width. Finite element models indicate that the pressure and the flow velocity at the mouth of the channel are high and that they may have an impact on the selectivity of the nano-device.

References

- Preston GM, Carroll TP, Guggino WB, Agre P (1992) Appearance of water channels in *Xenopus* oocytes expressing red-cell CHIP28 protein. *Science* 256:385–387
- Murata K, Mitsuoka K, Hirai T, Walz T, Agre P, Heymann JB, Engel A, Fujiyoshi Y (2000) Structural determinants of water permeation through aquaporin-1. *Nature* 407:599–605
- Tajkhorshid E, Nollert P, Jensen MØ, Miercke LJW, O’Connell J, Stroud RM, Schulten K (2002) Control of the selectivity of the aquaporin water channel family by global orientational tuning. *Science* 296:525–530
- Vidossich P, Cascella M, Carloni P (2004) Dynamics and energetic of water permeation through the aquaporin channel. *Proteins* 55: 924–931
- Aponte-Santamaria C, Fischer G, B ath P, Neutze R, de Groot BL (2017) Temperature dependence of protein-water interactions in a gated yeast aquaporin. *Sci. Rep.* 7(1):4016
- Saboe PO, Rapisarda C, Kaptan S, Hsiao YS, Summers SR, Zorzi RD, Dukovski D, Yu J, de Groot BL, Kumar M, Walz T (2017) Role of pore-lining residues in defining the rate of water conduction by aquaporin-0. *Biophys. J.* 112(14):953–965
- de Groot BL, Grubmuller H (2001) Water permeation across biological membranes: mechanism and dynamics of aquaporin-1 and GlpF. *Science* 294:2353–2357
- Lohrasebi A, Rafii-Tabar H (2008) Computational modeling of an ion-driven nanomotor. *Journal of Molecular Graphics and Modeling* 27:116–123
- Gong X, Li J, Lu H, Wan R, Li J, Hu J, Fang H (2007) A charge-driven molecular water pump. *Nature* 2:709–712
- Chen M, Zang J, Xiao D, Zhang C, Liu F (2009) Nanopumping molecules via a carbon nanotube. *Nano Res.* 2:938–944
- Lohrasebi A, Feshanjerdi M (2012) A rotary nano ion pump: a molecular dynamics study. *J. Mol. Model.* 18:4191–4197
- Rikhtehgaran S, Lohrasebi A (2015) Water desalination by a designed nano filter of graphene-charged carbon nanotube: a molecular dynamics study. *Desalination* 365:176–181
- Surwade SP, Smimov SN, Vlassioux IV, Unocic RR, Veith GM, Dai S, Mahurin SM (2015) Water desalination using nanoporous single-layer graphene. *Nat. Nanotechnol.* 10:459–464
- Wu K, Chen Z, Li J, Li X, Xu J, Dong X (2017) Wettability effect on nanoconfined water flow. *PNAS* 114:3358–3363
- Cohen-Tanugi D, Grossman JC (2015) Nanoporous graphene as a reverse osmosis membrane: recent insights from theory and simulation. *Desalination* 366:59–70
- Sun P, Wang K, Zhu H (2016) Recent developments in graphene-based membranes: structure. *Mass-Transport Mechanism and Potential Applications, Advanced Materials* 28:2287–2310
- Lohrasebi A, Rikhtehgaran S (2018) Ion separation and water purification by applying external electric field on porous graphene membrane. *Nano Res.* 11(4):2229–2236
- Cohen-Tanugi D, Lin LC, Grossman JC (2016) Multilayer nanoporous graphene membranes for water desalination. *Nano Lett.* 16:1027–1033
- Neek-Amal M, Lohrasebi A, Mousaei M, Radha B, Peeters FM (2018) Fast water flow through graphene nanocapillaries: a continuum model approach involving the microscopic structure of confined water. *Appl. Phys. Lett.* 113(8):083101–083106
- Kargar M, Khasheii F, Lohrasebi A (2018) Influence of electric fields on the efficiency of multilayer graphene membrane. *J. Mol. Model.* 24:241
- Qiu H, Zeng XC, Guo W (2015) Water in inhomogeneous nanoconfinement: coexistence of multilayered liquid and transition to ice nanoribbons. *ACS Nano* 9:9877–9884
- Joly L, Tocci G, Merabia S, Michaelides A (2016) Strong coupling between nanofluidic transport and interfacial chemistry: how defect reactivity controls liquid–solid friction through hydrogen bonding. *J. Phys. Chem. Lett.* 7(7):1381–1386
- Walther JH, Ritos K, Cruz-Chu ER, Megaridis CM, Koumoutsakos P (2013) Barriers to superfast water transport in carbon nanotube membranes. *Nano Lett.* 13(5):1910–1914
- Kargar M, Lohrasebi A (2019) Water flow modeling through the graphene-based nanochannel: theory and simulation. *Phys. Chem. Chem. Phys.* 21:3304–3309
- Chakraborty S, Kumar H, Dasgupta C, Maiti PK (2017) Confined water: structure, dynamics, and thermodynamics. *Acc. Chem. Res* 50(9):2139–2146
- Giri AK, Teixeira F, Nat alia M, Cordeiro DS (2019) Salt separation from water using graphene oxide nanochannels: a molecular dynamics simulation study. *Desalination* 460:1–14
- Giri AK, Teixeira F, Nat alia M, Cordeiro DS (2018) Structure and kinetics of water in highly confined conditions: a molecular dynamics simulation study. *J. Mole. Liq.* 268:625–636
- Cheng C, Jiang G, Garvey CJ, Wang Y, Simon GP, Liu JZ, Li D (2016) Ion transport in complex layered graphene-based membranes with tuneable interlayer spacing. *Sci. Adv.* 2:1501272
- Hong S, Constans C, Surmani Martins MV, Seow YC, Guevara Carri o JA, Garaj S (2017) Scalable graphene-based membranes for ionic sieving with ultrahigh charge selectivity. *Nano Lett.* 17: 728–732
- Zhou X, Wu F, Kou J, Nie X, Liu Y, Lu H (2013) Vibrating-charge-driven water pump controlled by the deformation of the carbon nanotube. *J. Phys. Chem. B* 117(39):11681–11686
- Wan X, Steudle E, Hartung W (2004) Gating of water channels (aquaporins) in cortical cells of young corn roots by mechanical stimuli (pressure pulses): effects of ABA and of HgCl₂. *J. Exp. Bot.* 55(396):411–422
- Abraham J, Vasu KS, Williams CD, Gopinadhan K, Su Y, Cherian CT, Dix J, Prestat E, Haigh SJ, Grigorieva IV, Carbone P, Geim AK, Nair RR (2017) Tuneable sieving of ions using graphene oxide membranes. *Nat. Nanotechnol.* 12(6):546–550
- Plimpton S (1995) Fast parallel algorithms for short-range molecular dynamics. *J. Comput. Phys.* 117:1–19

34. SJ Tuart, AB Tutein, JA Harrison (2000) A reactive potential for hydrocarbons with intermolecular interactions, *J. Chem. Phys.* 112, 6472–6486
35. Jorgensen WL, Chandrasekhar J, Madura JD, Impey RW, Klein ML (1983) Comparison of simple potential functions for simulating liquid water. *J. Chem. Phys.* 79:926–935
36. Allen M, Tildesley DJ (1987) *Computer simulation of liquids*. Oxford University Press, New York
37. COMSOL Multiphysics. Key: citeulike: 3255057
38. Conway BE (1981) *Ionic hydration in chemistry and biophysics*. Elsevier Science, Ltd.
39. Zeidel ML, Ambudkar SV, Smith BL, Agre P (1992) Water permeability of asymmetric planar lipid bilayers. *Biochemistry* 31:7436–7440
40. Kumar M, Grzelakowski M, Zilles J, Clark M, Meier W (2007) Highly permeable polymeric membranes based on the incorporation of the functional water channel protein Aquaporin. *Z. Proc. Natl Acad. Sci.* 104:20719–20724
41. Geng, J. et al. Stochastic transport through carbon nanotubes in lipid bilayers and live cell membranes. *Nature* 514, 612–615 (2014)
42. Tunuguntla RH et al (2017) Enhanced water permeability and tunable ion selectivity in subnanometer carbon nanotube porins. *Science* 357:792–796
43. Garaj S, Hubbard W, Reina A, Kong J, Branton D, Golovchenko JA (2010) Graphene as a subnanometre trans-electrode membrane. *Nature* 467:190–194

Publisher's note Springer Nature remains neutral with regard to jurisdictional claims in published maps and institutional affiliations.